ЖУРНАЛ СТРУКТУРНОЙ ХИМИИ

2015. Том 56, № 4 *Июль* *С. 656 – 666*

UDC 541.6:546.21:546.92

A DENSITY FUNCTIONAL THEORY ANALYSIS OF THE MOLECULAR HYDROGEN DISSOCIATION ON Al_nPt (n = 1—12) CLUSTERS

X. An, L. Guo, N. Ren, C. Wen, X. Dong, S. Niu

School of Chemistry and Materials Science, School of Modern Arts and Sciences, Shanxi Normal University, Linfen, P. R. China
E-mail: gl-guoling@163.com

Статья поступила 12 января 2014 г.

Bimetallic alloys are considered to be a promising type of catalysts with improved activity and selectivity that are distinct from those of the corresponding pure nanoclusters [1—4]. Using first principles density functional calculations, we study the structures and energies of Al_nPt bimetallic clusters up to 13 atoms. If platinum, nickel, and other transition metal catalysts are particularly important in the catalysis of hydrogen, hydrogen adsorption on a metal surface is an important step in the catalytic reaction. Because of large exothermic energy changes and relatively small activation energies, Al_7Pt and $Al_{12}Pt$ could serve as highly efficient and low-cost catalysts for the hydrogen dissociation. To clarify this assumption and achieve a good understanding, the H_2 adsorption and dissociation over bimetallic AlPt clusters are systematically investigated in our work.

DOI: 10.15372/JSC20150402

K e y w o r d s: Al_nPt bimetallic cluster, hydrogen adsorption, DFT calculations, dissociation mechanism.

INTRODUCTION

Bimetallic alloy surfaces are promising candidates for designing heterogeneous catalysts because of the possibility to control the surface electronic and geometric structures determining the reactivity [5—9]. Platinum, which is well known for the catalytic properties, is often used as a catalyst in different fuel cells [10—12]. Some success has been reported with Pt alloys [13—16] which may help to reduce the catalyst cost. Thus, recent experimental and theoretical efforts in electrocatalysis have been focused on designing and testing new materials to increase the catalytic activity using less expensive materials. By the plasma—gas—condensation (PGC) method, Peng et al. studied the structure and magnetic properties of FePt alloy cluster-assembled films [17]. Benguedouara et al. have examined the structural and magnetic properties of Ni—Pt nanoalloys supported on silica, which indicates that platinum seems to play a major role by enhancing the nickel ion reduction and protecting Ni against corrosion during the synthesis [18].There are some reports on the adsorbed gas molecules in the clusters. CO adsorption on Pt—Au nanoparticles have been studied by Song et al. using the density functional theory approach [19]. Huang et al. studied the local electronic alloy effects of OOH, OH, and O adsorption within the Pt—Pd cluster model [20]. Chen et al. have studied the oxygen adsorption in Au→Pt/Pt(111) surface alloys [21]. H_2O dissociation on bimetallic Pt/Ru nanoclusters has been studied by Ishikawa et al. [22]. Piotrowski et al. have investigated the NO adsorption on Rh_{13}, Pd_{13}, Ir_{13}, and Pt_{13} clusters [23].

As compared with the widely studied clusters such as palladium, zirconium, and gold, aluminum is a common and cheap metal with a lighter mass. Especially, aluminum alloy clusters provide a matter of increasing interest in pure and applied materials sciences and the traditional fields of physics and chemistry. However, pure Al_n clusters do not adsorb hydrogen similarly to the Al bulk phase behavior. The penetration of transition metal can improve the adsorption properties of hydrogen storage materials. For aluminum transition alloy clusters, we are unaware of many systematic experimental and theoretical studies on the hydrogen adsorption. Tarakeshwar et al. [24] carried out the *ab initio* calculations of the hydrogen saturation of bimetallic titanium—aluminum nanoclusters. Huang et. al. [25] studied the reactive adsorption of hydrogen molecules of neutral $Y_mSi@Al_{12}$ clusters. In this study, they found that the doping of $Si@Al_{12}$ clusters with Y atoms reveals a remarkable increase in hydrogen adsorption rates as compared to pure $Si@Al_{12}$ clusters.

We were inspired by the adsorption capabilities of aluminum transition alloy clusters. In our recent work, we presented the extensive calculations of the physical and chemical adsorption of hydrogen loading on the energetically stable Al_nPt clusters and provide a detailed picture on the Al_nPt alloy cluster via examining the reaction energy, activation barrier, and reaction mechanisms for the H_2 physisorption and dissociative chemisorption. H_2 is easily absorbed physically on the top Pt atom of Al_nPt clusters with an end-on orientation rather than with a side-on orientation because of the more effective orbital overlap in the end-on orientation. The reaction of Al_nPt with H_2 would produce Al_nPtH_2 because of large exothermic energy changes and relatively small activation energies, which could serve as highly efficient and low-cost catalysts for the hydrogen dissociation. To our knowledge, this is the first time that a systematic study of the hydrogen adsorption and dissociation on small Al_nPt clusters (n = 1—12) has been performed.

METHODOLOGY

The calculations were carried out within the DFT framework with the generalized gradient approximation (GGA) implemented in the Gaussian 03 program [26]. Full optimized structures and normal-mode frequencies are found using the hybrid B3LYP functional [27]. The LANL2DZ pseudopotential is adopted for the valence electrons of the Pt atom, and its core electrons are represented by the LANL2DZ effective core potential (ECP). The standard 6-31G* basis set was used for oxygen and carbon atoms. All of the vibrational frequencies have been calculated using the analytic second derivatives of the energy to judge whether the structure was a local minimum. The quadratic synchronous transit (QST) method [28] is used to determine the transition state (TS) geometries. All the structures are fully optimized without any constraints. For the reaction pathways, the minima are related to each TS by tracing the intrinsic reaction coordinate (IRC) [29].

The number of distinct initial geometries is important for the reliability of the obtained lowest energy structures. We selected the initial structures by following three ways: first, by considering the configurations of the Al_n clusters available from the previous studies [30]. We have considered possible isomeric structures by placing the Pt atom on each possible site of the Al_n cluster. Second, we substituted one Al atom by the Pt atom from the Al_{n+1} cluster. Third, other Al_nX (X = Cu, Au, Co, ect.) stable isomers [31] were also considered as candidates. The equilibrium geometries of the Al_nPt clusters were optimized, and their stabilities were accurately assessed by the harmonic vibrational frequency calculation that also provided zero-point vibrational energy (ZPE) corrections without the imaginary mode. Further, different spin multiplicities of the low-lying energy isomers were analyzed. We considered an increasingly higher spin state until the energy minimum with respect to spin multiplicity was reached. Therefore, all isomers of this cluster are surely the local minima.

RESULTS AND DISCUSSION

Structures of the Al_nPt (n = 1—12) clusters. In cluster physics, one of the most fundamental problems is to determine the ground state geometry. Accordingly, we first studied the ground state structures of Al_nPt clusters shown in Fig. 1(*na*). Multiplicity(M), symmetries (Sym), HOMO—LUMO gap (Gap), atomic averaged binding energy (E_b), the second-order energy differences (Δ_2E), vertical

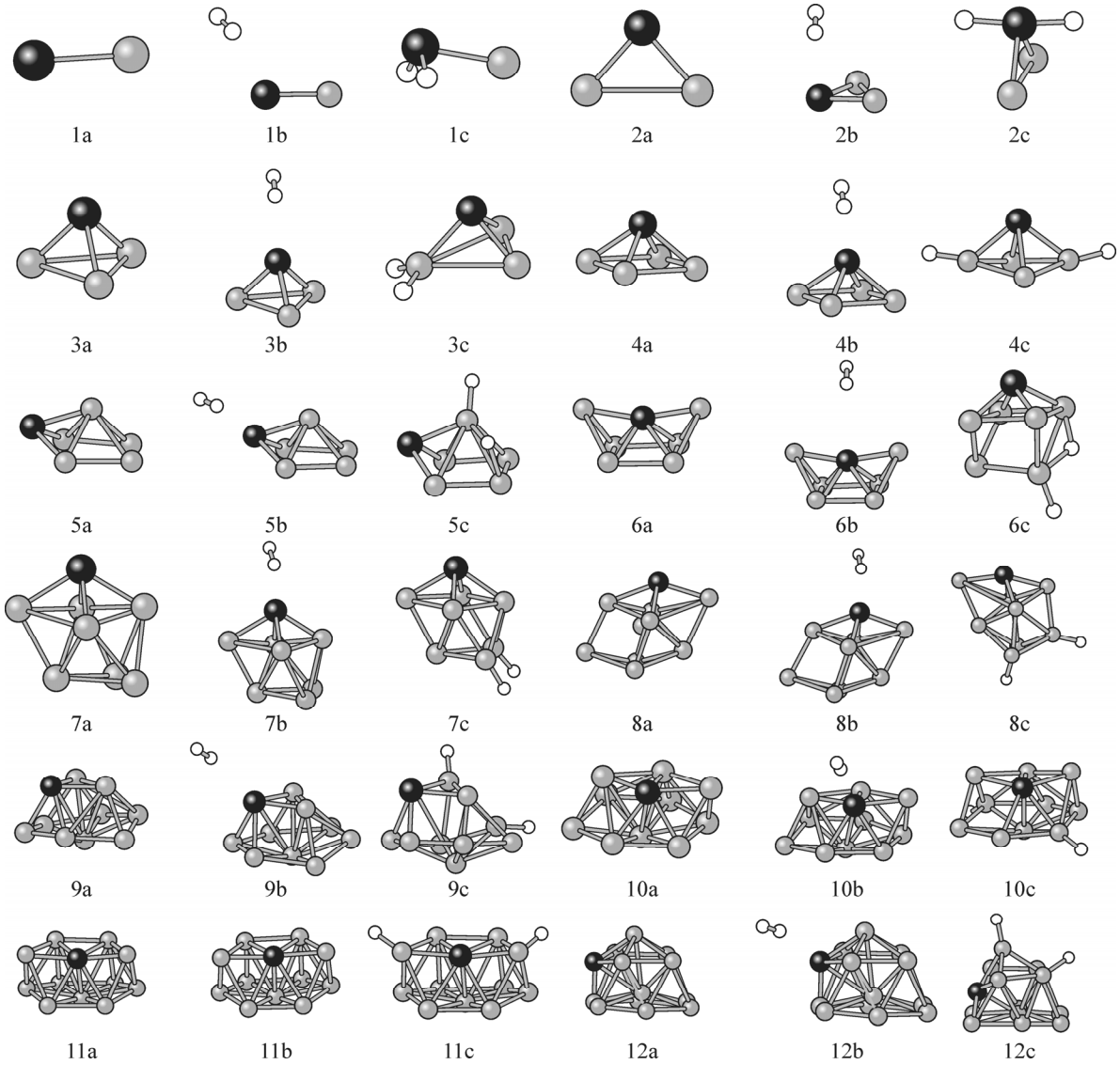

Fig. 1. The lowest energy structures of Al_nPt (*na*), $Al_nPt—H_2$ (*nb*), and Al_nPtH_2 (*nc*).
Black, gray, and white balls are used for Pt, Al, and H respectively

ionization potential (VIP), and vertical electron affinities (VEA) (all in eV) for the most stable Al_nPt clusters are all shown in Table 2.

The predicted ground state spin multiplicity for AlPt [Fig. 1, 1a] is found to be a doublet. The singlet Al_2Pt cluster is an isosceles triangle with the C_{2v} symmetry [Fig. 1, 2a], in which the Pt atom is

T a b l e 1

Calculated bond lengths, averaged binding energies, and vertical ionization potentials, experiment results, and theoretical results of this study

	Pt_2		Al_2	
	This work	Experimental [21]	This work	Experimental [22]
Bond length, Å	2.376	2.330	2.514	2.560
Ionization potential, eV	8.444	8.800±0.200	6.294	6.200±0.200
E_b, eV	1.288	1.570±0.020	1.170	0.997±0.108

Table 2

Multiplicity (M), *symmetries* (Sym), HOMO—LUMO *gaps* (Gap), *averaged binding energies* (E_b), *second-order energy differences* (Δ_2E), *vertical ionization potentials* (VIP), *and vertical electron affinities* (VEA) (*all in* eV) *for the most stable* Al_nPt (n = 1—13) *clusters*

Cluster	M	Sym	Gap	E_b	Δ_2E	VIP	VEA
AlPt(1*a*)	2	$C_{\infty v}$	3.622	1.723		7.600	1.976
Al_2Pt(2*a*)	1	C_{2v}	2.960	2.392	1.769	7.325	0.844
Al_3Pt(3*a*)	2	C_{3v}	1.489	2.285	0.544	5.850	1.162
Al_4Pt(4*a*)	3	C_{4v}	1.839	2.111	–0.264	5.987	1.630
Al_5Pt(5*a*)	2	C_s	1.583	2.044	–0.789	6.202	1.766
Al_6Pt(6*a*)	1	C_{2v}	1.761	2.103	–0.014	6.302	1.820
Al_7Pt(7*a*)	2	C_1	1.520	2.153	0.593	6.063	1.799
Al_8Pt(8*a*)	1	C_s	1.714	2.128	–0.147	6.188	1.818
Al_9Pt(9*a*)	2	C_1	1.461	2.122	–0.082	6.150	2.435
$Al_{10}Pt$(10*a*)	1	C_1	1.260	2.125	–0.351	6.123	2.378
$Al_{11}Pt$(11*a*)	2	C_1	1.579	2.156	0.220	5.864	2.316
$Al_{12}Pt$(12*a*)	1	C_1	1.410	2.166		6.123	2.343

at the apex of Al_2 cluster [30c]. The lowest energy structure of Al_3 is an equilateral trianglur structure with the D_{3h} symmetry [30c]. When we move to Al_3Pt, the three-dimensional structure takes over. The Al_3Pt cluster takes a spin doublet tetrahedron [Fig. 1, 3a] with the C_{3v} symmetry, in which the Pt atom sits on the hallow site of triangular Al_3 and forms a pyramidal structure. Al_4 is a square with the D_{4h} symmetry [30c]. The Al_4Pt takes the pyramidal (C_{4v}) structure [Fig. 1, 4a] with a spin triplet as its ground state, in which the Pt atom occupies the top position of Al_4 [30c]. For the spin doublet Al_5Pt [Fig. 1, 5a], the Pt atom capped pyramidal structure of Al_5 is the lowest energy configuration. The lowest energy isomer of Al_6Pt is a spin singlet structure [Fig. 1, 6a] with the C_{2v} symmetry, which can be seen as two Al atoms capping Al_4Pt. For Al_7Pt, the ground-state structure is a spin doublet with the C_1 symmetry [Fig. 1, 7a], which can be seen as the Pt atom occupying the top position of Al_7 [19c]. Al_8Pt has a spin singlet with the C_s symmetry [Fig. 1, 8a], which can also be seen as a Pt atom occupying the top position of Al_8 [30c]. The lowest energy structure for Al_9Pt is the spin doubelt structure with the C_1 symmetry [Fig. 1, 9a]. The growth pattern of $Al_{10}Pt$ and $Al_{11}Pt$ is different from the above clusters. The lowest energy isomer of $Al_{10}Pt$ and $Al_{11}Pt$ are the spin singlet structure [Fig. 1(10a] with the C_1 symmetry and the spin doublet structure with the C_1 symmetry [Fig. 1, 11a], which can be seen as the Pt atom substituting for one Al atom of Al_{11} and Al_{12} [30c]. Just as in the Al_nPt (n = 2, 3, 4, 7, and 8) cluster, the ground state geometry of $Al_{12}Pt$ [Fig. 1, 9a] is the Pt atom occupying the peripheral site of the Al_{12} cluster [30c].

In summary, the growth pattern for Al_nPt (n = 2—4, 7, 8, and 12) clusters is the Pt atom occupying a peripheral position of the Al_n clusters [30c], and the growth pattern for the Al_nPt (n = 10 and 11) clusters is the Pt-substituted Al_{n+1} clusters. It is found that the Pt atom substitutes for the surface atom of the Al_{n+1} cluster and occupies a peripheral position. The structures of Al_5Pt, Al_6Pt, and Al_9Pt do not meet the above rule.

Adsorption of an H_2 molecule on Al_nPt (n = 1—12) clusters. We study the physisorption of an H_2 molecule on the Al_nPt clusters by DFT calculations with the B3LYP correlation functional. Three kinds of adsorption sites, i.e., top, edge and face, are considered, and the most stable adsorption modes are shown in Fig. 1(*nb*). The adsorption energy, HOMO—LUMO gap, H—H bond length, and H—Pt distance are summarized in Table 3. The adsorption energy is evaluated using the equation

$$\Delta E_{ad} = E(Al_nPt) + E(H_2) - E(Al_nPtH_2),$$

where $E(Al_nPt)$, $E(H_2)$, and $E(Al_nPtH_2)$ are the calculated lowest energies of the Al_nPt clusters, H_2

Table 3

Adsorption energy [ΔE_{ad}, eV], HOMO—LUMO *gaps* [Gap, eV], H—H *bond lengths* [$D_{H—H}$, Å], *averaged* H—Pt *bond lengths* [$D_{H—V}$, Å], *and* H—H *vibrational frequencies* [ω, cm^{-1}] *for* H_2 *physisorption on the* Al_nPt (n = 1—13) *clusters*

Cluster	ΔE_{ad}	Gap	$D_{H—H}$	$D_{H—Pt}$	ω	Cluster	ΔE_{ad}	Gap	$D_{H—H}$	$D_{H—Pt}$	ω
AlPt—H_2 (1b)	–0.280	3.548	0.751	2.876	4261	Al_7Pt—H_2 (7b)	0.014	1.519	0.746	3.336	4390
Al_2Pt—H_2 (2b)	0.027	2.976	0.746	3.507	4383	Al_8Pt—H_2 (8b)	0.016	1.703	0.745	3.395	4394
Al_3Pt—H_2 (3b)	0.019	1.489	0.745	3.610	4404	Al_9Pt—H_2 (9b)	0.008	1.458	0.746	3.268	4382
Al_4Pt—H_2 (4b)	0.011	1.839	0.744	3.950	4424	$Al_{10}Pt$—H_2 (10b)	0.014	1.260	0.745	3.500	4399
Al_5Pt—H_2 (5b)	0.016	1.583	0.745	3.435	4397	$Al_{11}Pt$—H_2 (11b)	0.011	1.579	0.744	4.100	4438
Al_6Pt—H_2 (6b)	0.008	1.760	0.744	4.125	4445	$Al_{12}Pt$—H_2 (12b)	0.019	1.408	0.745	3.650	4406

molecule, and the hydrogen molecule adsorbed on the Al_nPt clusters (negative ΔE_{ad} means the exothermic process, whereas positive ΔE_{ad} means the endothermic process). It is noted that the most favored adsorption site for most clusters is on the Pt top site, which results from the low coordination of Pt atoms placed on the top sites, such as the H_2 adsorption on the lowest coordination atoms in $(ZrO_2)_n$ [31] clusters. It is attributed to the unsaturated coordinate. It is worth noting that the H_2 molecule approaches Al_nPt with an end-on orientation rather than a side-on orientation.

When an H_2 molecule is physisorbed on the Al_nPt clusters, the H—H bond length expands slightly. This result indicates that the H—H bond has a relaxation on the Al_nPt clusters, which is similar to the H_2 adsorption on the $(ZrO_2)_n$ [32] and Au [36] clusters. In [33], the adsorption energy (including ZPE correction) for the H_2 physisorption on $Al_{12}X$ (X = B, Al, C, Si, P, Mg, and Ca) is about 0.03—0.04 eV within the general gradient approximation (GGA) with the Perdew and Wang (PW91) functional and the double numerical basis set including *p*- and *d*-polarization (DNP). Lu′s calculation [34] makes clear that the adsorption energies of H_2 on Si@Al_{12} and Sc-coated Si@Al_{12} are less than 0.01 eV and 0.276 eV respectively with the Perdew—Burke—Ernzerhof (PB*E*) functional based on the generalized approximation (GGA). For comparison, our results of the adsorption energies of H_2 physisorption on Al_nPt (n = 1—12) clusters are 0.008—0.280 eV. In addition, the distance between the H_2 molecule and the Al_nPt clusters ranges from 2.876 Å to 4.125 Å, which is typical of van der Waalls interactions. The H—H lengths are a little longer than those of the isolated H_2 molecule (0.743 Å), which all illustrats that their adsorption is the nature of the physical adsorption.

The vibrational frequencies of H_2 on the Al_nPt clusters are also investigated. The H—H symmetric stretching vibrational frequency in Al_nPt—H_2 is in the range of 4261—4445 cm^{-1}, while it is around 4650 cm^{-1} in the gaseous H_2 molecule. The H—H vibrational frequency shifts to low wave numbers after H_2 adsorption, which is similar to the trend of H_2 on $(ZrO_2)_n$ [31] clusters. This H—H vibrational frequency shift in the adsorbed clusters is attributed to an increase in the H—H bond length.

Chemisorption of H_2 on Al_nPt (n = 1—12) clusters. Another motive of our current work is to investigate hydrogen chemisorptions on the small Al_nPt (n = 1—12) clusters. We performed an exhaustive minimum energy structural search for H chemisorptions on the optimized bare Al_nPt (n = 1—12) clusters with lowest energy structures. The possibility that the Al_nPtH_2 isomer does not come from the most stable Al_nPt cluster has also been investigated. Our investigation shows that the most stable Al_nPtH_2 complexes (except for n = 6) always come from those of the lowest energy bare Al_nPt cluster plus the attached H atoms. When two individual hydrogen atoms are chemisorbed on Al_nPt clusters, the equilibrium structures are found for the Al_nPtH_2 complex (Fig. 1(*n*c). In Table 4, the multiplicity (M), symmetries (Sym), H—H bond lengths [$D_{H—H}$ (Å)], HOMO—LUMO gaps (Gap), averaged binding energy (E_b), the second-order energy differences ($\Delta_2 E_n$), vertical ionization potential (VIP), and vertical electron affinities (VEA) (all in eV) of the most stable Al_nPtH_2 (n = 1—12) clusters are shown. When H_2 approaches AlPt with the H—H bond perpendicular to the Pt atom, it dissociates with both H atoms adsorbed on the top position (Fig. 1, 1c).

Table 4

Multiplicity (M), *symmetries* (Sym), H—H *bond lengths* [$D_{H—H}$, Å], HOMO—LUMO *gaps* (Gap), *averaged binding energies* (E_b), *chemisorption energy* (ΔE_{CE}), *second-order energy differences* ($\Delta_2 E_n$), *vertical ionization potentials* (VIP), *and vertical electron affinities* (VEA) (*all in* eV) *of the most stable* Al_nPtH_2 (n = 1—13) *clusters. Location of* H *is represented by symbols* h, n, o, b, t *which mean hollow*, *neighboring*, *opposite*, *bridging*, *and top sites*, *respectively*

Cluster	Location of H	M	Sym	$D_{H—H}$	Gap	E_b	$\Delta_2 E_n$	VIP	VEA
$AlPtH_2$ (1c)	t, t (Pt)	2	C_s	2.876	3.222	2.148		8.068	1.663
Al_2PtH_2 (2c)	t, t (Pt)	1	C_{2v}	3.338	3.522	2.424	1.570	8.125	1.064
Al_3PtH_2 (3c)	t, t (Al)	2	C_1	2.731	1.762	2.345	0.555	6.400	1.529
Al_4PtH_2 (4c)	o, t (Al, Al)	3	C_{2v}	7.142	2.465	2.210	–0.571	6.539	1.731
Al_5PtH_2 (5c)	t (Al), b (Al, Pt)	2	C_1	2.666	1.787	2.491	–0.493	6.378	2.000
Al_6PtH_2 (6c)	t (Al), b (Al, Pt)	1	C_1	2.679	1.851	2.211	–0.389	6.479	1.820
Al_7PtH_2 (7c)	n, t (Al, Al)	2	C_1	4.634	1.816	2.276	1.235	6.329	2.340
Al_8PtH_2 (8c)	n, t (Al, Al)	1	C_1	4.881	1.697	2.215	–0.577	6.270	1.937
Al_9PtH_2 (9c)	n, t (Al, Al)	2	C_1	4.619	1.771	2.214	0.0082	6.155	2.400
$Al_{10}PtH_2$ (10c)	o, t (Al, Al)	1	C_1	7.991	1.655	2.211	–0.054	6.204	2.065
$Al_{11}PtH_2$ (11c)	o, t (Al, Al)	2	C_s	7.193	1.786	2.213	–0.239	6.311	2.691
$Al_{12}PtH_2$ (12c)	n, t (Al, Al)	1	C_1	4.531	1.828	2.231		6.329	2.180

Our results show that the configuration with two H atoms bound on the top site of Pt is the most stable geometry of Al_2PtH_2 (Fig. 1, 2c). Two H atoms on the top site of one Al atom of the Al_3Pt tetrahedron form the lowest energy geometry of Al_3PtH_2 (Fig. 1, 3c). Two H atoms on the top sites of two neighboring Al atoms of Al_7Pt, Al_8Pt, Al_9Pt, and $Al_{12}Pt$ form the lowest energy geometry of Al_7PtH_2 [Fig. 1, 7c], Al_8PtH_2 [Fig. 1, 8c], Al_9PtH_2 (Fig. 1, 9c), and $Al_{12}PtH_2$ (Fig. 1, 12c), which is regarded as the conventionally adsorbed configuration and identical to the result obtained by Wang et al. [31] and Yarovsky et al. [36]. In addition, the adsorption of two hydrogen atoms on two opposite top sites of the Al atoms constitute the ground state structure of Al_4PtH_2 (Fig. 1, 4c), $Al_{10}PtH_2$ (Fig. 1, 10c), and $Al_{11}PtH_2$ (Fig. 1, 11c). For Al_5PtH_2 (Fig. 1, 5c) and Al_6PtH_2 (Fig. 1, 6c), new alternative configurations are found, in which one H atom is located at the top site of the Al atom and another H atom takes the bridge adsorption with the neighboring Al and Pt atoms.

The distances between two hydrogen atoms on Al_nPt in the lowest energy states range from 2.666 Å to 7.991 Å (Table 4) as compared to the calculated bond length of 0.743 Å in H_2. Accordingly, hydrogen is likely to be dissociated on Al_nPt clusters.

Comparison of properties for Al_nPt and Al_nPtH_2. Now we discuss the relative stability of Al_nPt and Al_nPtH_2 clusters by computing the energy indicative of the stability. We computed the average binding energy (E_b) per atom and the second-order energy differences ($\Delta_2 E$) respectively. The second-order energy differences ($\Delta_2 E$) are sensitive quantities that reflect the relative stability of the investigated clusters. The $\Delta_2 E$ value is often compared directly with relative abundances determined in mass spectroscopy experiments. A larger positive $\Delta_2 E$ value indicates that the previous size of the clusters forming the size clusters emits more energy, while in the formation of the next size clusters more energy is needed. The larger the value, the better the corresponding structural stability is.

$$E_b[Al_nPt] = (nE[Al] + E[Pt] - E[Al_nPt]/(n + 1) \quad (1)$$

$$E_b[Al_nPtH_2] = (nE[Al] + E[Pt] + E[H_2] - E[Al_nPtH_2]/(n + 1) \quad (2)$$

$$\Delta_2 E[Al_nPt] = E[Al_{n+1}Pt] + E[Al_{n-1}Pt] - 2E[Al_nPt] \quad (3)$$

$$\Delta_2 E[Al_nPtH_2] = E[Al_{n+1}PtH_2] + E[Al_{n-1}PtH_2] - 2E[Al_nPtH_2]. \quad (4)$$

In general, the E_b value increases sharply for very small clusters and then a plateau follows as the cluster size grows. Small humps or dips for the specific cluster size signify their relative stabilities.

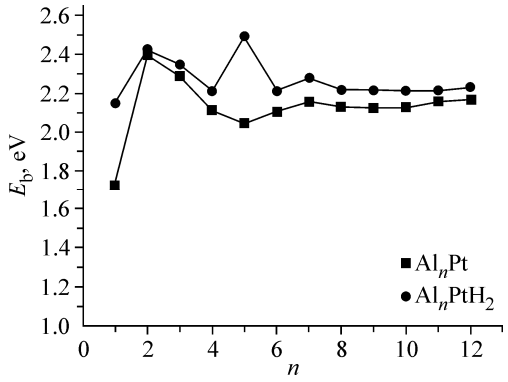

Fig. 2. Size dependence of the average binding energy of the lowest energy Al_nPt and Al_nPtH_2 clusters

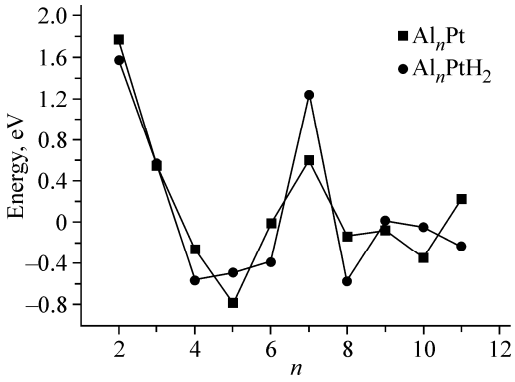

Fig. 3. Size dependence of the second-order energy difference of the lowest energy Al_nPt and Al_nPtH_2 clusters

The larger binding energy, the stronger adsorption is. From the average binding energy curves for Al_nPt and Al_nPtH_2 clusters given in Fig. 2, Table 2, and Table 4, we see that as we go from Al_nPt to Al_nPtH_2 clusters the binding energies go up from the range 1.723—2.166 eV to the range 2.148—2.231 eV. This shows the greater stability of Al_nPtH_2 as compared to Al_nPt. For Al_nPt and Al_nPtH_2 the maximum of the E_b values are Al_2Pt and Al_5PtH_2, the minimum values of those are AlPt and $AlPtH_2$, respectively. Small humps (Al_2Pt, Al_2PtH_2, and Al_5PtH_2) for the specific cluster size signify their relative stabilities. Both Al_nPt and Al_nPtH_2 clusters attain stability more quickly, which may indicate an approach to the stationary bulk regime.

In cluster physics, the second-order energy differences (Δ_2E) are sensitive quantities that reflect the relative stability of the investigated clusters. The Δ_2E value is often compared directly with the relative abundances determined in mass spectroscopy experiments. As shown in Fig. 3, Table 2, and Table 4, the particularly prominent maximum Δ_2E values of pure Al_nPt are found at $n = 2$, 7, and 11, indicating higher stability than that of their neighboring clusters. In the case of Al_nPtH_2, the cluster sizes $n = 2$ and 7 are the most stable ones. By comparing the Δ_2E_n values for the Al_nPt and Al_nPtH_2 clusters, both values follow the same trend. From Fig. 3, we can also find that the Δ_2E_n values of $n = 5$, 7, and 10 become higher; $n = 2$, 4, 6, 8, and 11 become smaller after hydrogen chemisorptions.

Experimentally, the electronic structure is probed via measurements of ionization potentials, electron affinities, polarizabilities, etc. Therefore, we also studies these quantities (Fig. 4, Table 2, and Table 4) to understand their evolution with size. The vertical ionization potential (VIP) is calculated as the self-consistent energy difference between the cluster and its positive ion with the same geometry. We have also calculated the vertical electron affinities (VEA) for these clusters by assuming the geometry of the charged cluster to be the same as of the neutral one. In general, both VIPs decrease as the clusters grow with the local maxima for AlPt, Al_6Pt, Al_2PtH_2, for which it is difficult to remove an electron. Fig. 4 shows that the VEA values of both Al_nPt and Al_nPtH_2 clusters show the same variation tendency, that is, increase as the number of atoms increases and exhibit strong even-odd alternations with the local minimum at odd-numbered clusters. It is interesting to point out that the large-sized clusters usually have smaller VIPs and larger VEAs as compared to the small-sized clusters, implying that it is much more difficult to ionize the smaller clusters than the larger ones but much easier to attach an electron to the larger clusters than to the smaller ones.

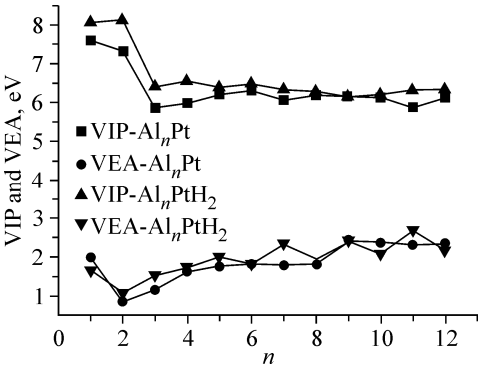

Fig. 4. Size dependence of VIPs and VEAs of the lowest energy Al_nPt and Al_nPtH_2 clusters

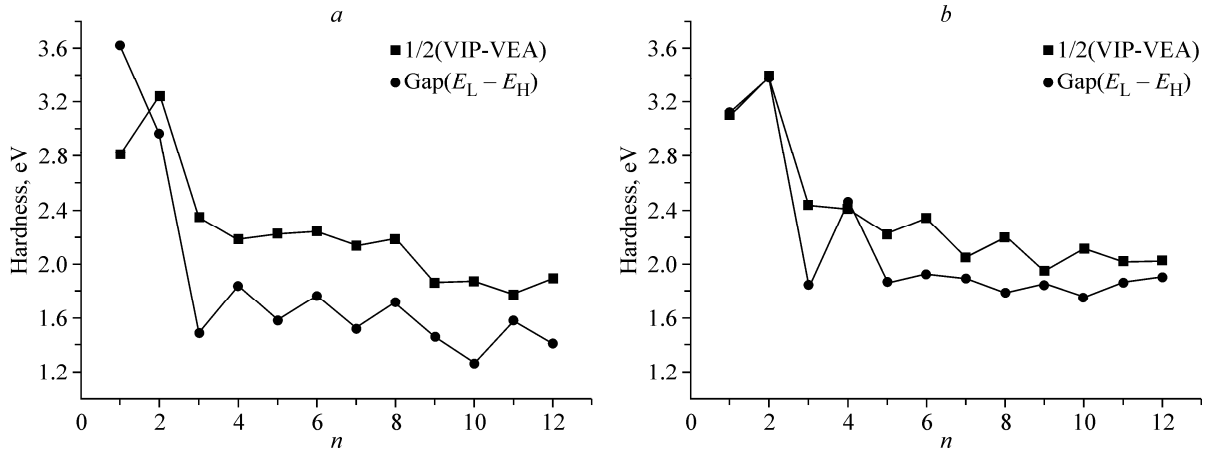

Fig. 5. Size dependence of the chemical hardness and the HOMO-LUMO gap of Al_nPt (*a*) and Al_nPtH_2 (*b*) clusters

Moreover, the calculated VIPs and VEAs of each cluster can be used to describe the chemical hardness of the clusters, according to the definition of hardness from Parr and Pearson [35, 36]. The hardness of the ground state of Al_nPt and Al_nPtH_2 is depicted in Figs. 5, *a* and 5, *b*, respectively. They are calculated in two different ways: first, as the difference between the VIP and electron affinity and second, as the difference between the LUMO and HOMO energies. Both values follow the same trend. In comparing the hardness for the two families of the Al_nPt and Al_nPtH_2 clusters, it is observed that there is correlation between them, which can explain small changes in the geometrical structure when the hydrogen atoms are added.

H_2 dissociation mechanism on Al_nPt (n = 1—12) clusters. To examine the H_2 dissociative process on Al_nPt (n = 1—12) clusters, we consider the Al_nPt clusters as physisorbed and chemisorbed with an H_2 molecule as the reactant and product, respectively. The computed reaction energy (ΔE_0, including the zero-point energy correction (kcal/mol), the activation barrier (kcal/mol), the imaginary frequency of the transition state (ω (cm^{-1})), and the H—H bond length of the transition state ($D_{H—H}$ (Å)) at the transition from the physisorbed $Al_nPt—H_2$ cluster to the related chemisorbed form are summarized in Table 5. The reaction energy (ΔE_0) is directly calculated by the total energy difference between the reactant and the product (a negative ΔE_0 value means an exothermic process, whereas a positive ΔE_0 value means an endothermic process). The activation barrier is calculated by the total energy difference between the reactant and the transition state (TS). TS for the H_2 dissociation on the Al_nPt clusters are then located using the TS search methodology described previously. Each TS has only one large imaginary frequency, indicating that we have located true TS.

In summary, the H_2 dissociation on all Al_nPt clusters is exothermic as identified by the negative reaction energies (ca. –8.911 to –24.473 kcal/mol). Among them, Al_7Pt and $Al_{12}Pt$ clusters have the

T a b l e 5

Reaction energy ΔE_0, *including the zero-point energy correction* (kcal/mol)], *activation barriers* (kcal/mol), TS *imaginary frequencies* [ω, cm^{-1}], and the H—H bond length of TS [$D_{H—H}$, Å] *for the transition from the physisorbed* $Al_nPt—H_2$ *cluster to the related chemisorbed form*

Cluster	ΔE_0	Activation Barrier	ω	$D_{H—H}$	Cluster	ΔE_0	Activation Barrier	ω	$D_{H—H}$
AlPt	–8.911	4.832	–939	1.200	Al_7Pt	–24.473	19.516	–850	1.372
Al_2Pt	–11.232	33.195	–980	2.002	Al_8Pt	–17.445	17.319	–1085	1.281
Al_3Pt	–10.856	26.669	–1152	1.246	Al_9Pt	–20.080	23.218	–785	0.993
Al_4Pt	–10.291	18.825	–1091	1.276	$Al_{10}Pt$	–20.959	15.625	–1120	1.187
Al_5Pt	–17.006	17.696	–1088	1.123	$Al_{11}Pt$	–14.809	25.602	–1141	1.199
Al_6Pt	–12.613	24.598	–1169	1.133	$Al_{12}Pt$	–19.453	7.656	–1123	1.160

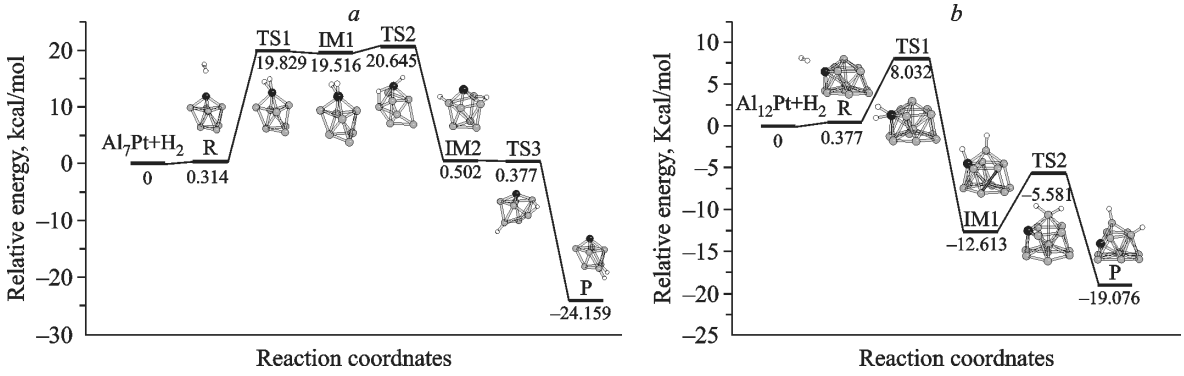

Fig. 6. Dissociation reaction pathway and energetic barriers of H_2 on the Al_nPt (n = 7 and 12) clusters

larger (negative) reaction energies (–24.473 kcal/mol for Al_7Pt, –19.435 kcal/mol for $Al_{12}Pt$) and the lower activation barriers (19.516 kcal/mol for Al_7Pt, 7.656 kcal/mol for $Al_{12}Pt$). Thus, Al_7Pt and $Al_{12}Pt$ exhibit significant chemical reactivities and are able to break the H—H bond exothermically when interacting with an H_2 molecule. On the other hand, Al_2Pt and Al_3Pt possess the high activation barriers (33.195 kcal/mol for Al_2Pt, 26.669 kcal/mol for Al_3Pt).

Wang et al. [31] investigated the H_2 molecule dissociation on the doped icosahedral $Al_{12}X$ (X = B, Al, C, Si, P, Mg, and Ca) clusters at the density functional theory level. We have also calculated the potential energy surfaces (PESs) for the dissociative chemisorption reactions $H_2 + Al_{12}Pt \rightarrow Al_nPtH_2$. The representative PESs of Al_7Pt and $Al_{12}Pt$ are indicated in Fig. 6, *a*, *b*. For Al_nPt (n = 7 and 12), the dissociation mechanism of H_2 on the top sites has been studied, and intermediates (IMs) and TSs have been searched. The geometry of TSs and IMs along with the energy barriers are shown in Fig. 6. The stable adsorption configuration of Fig. 1, 7b and 12b) was chosen as the initial reactants (R) for the TS search. These structures are energetically more favored by 0.314 kcal/mol and 0.438 kcal/mol than those of the free H_2 and Al_nPt reactants (n = 7 and 12), respectively. In the R complex, the H—H bond lengths are 0.745 Å and 0.746 Å, being only by 0.002 Å and 0.003 Å longer than the H—H bond length of the isolated H_2 molecule (0.743 Å).

The H_2 dissociation path of Al_7Pt and $Al_{12}Pt$ from R to IM undergo TS, overcoming the energy barrier of 19.516 kcal/mol and 7.656 kcal/mol, respectively. In TS, the H—H bond is split with an H—H bond lengths of 1.372 Å and 1.160 Å. TS has only one imaginary frequency, which is –850 cm^{-1} and –1123 cm^{-1} (Table 5).

In IM1 of the Al_7Pt cluster, two H atoms are bound to the top site of the Al atom with H—Al bond lengths of 1.610 Å and 1.625 Å, respectively. For IM of the $Al_{12}Pt$ cluster, one H atom is bound to the top site of the Pt atom with an H—Pt bond length of 1.633 Å, and another H atom is adsorbed on the Al atom with the H—Al distance of 1.580 Å. Conversion from IM1 (IM) to more stable IM2 (P) proceeds through TS2 with energy barriers of 1.129 kcal/mol and 7.032 kcal/mol, respectively, for the Al_7Pt and $Al_{12}Pt$ clusters. For Al_7Pt, IM2 further evolves into P along the reaction coordinate. The saddle point connecting IM2 and P is TS3 with an imaginary frequency of 163.3 cm^{-1}. The overall dissociation and diffusion processes of Al_nPt (n = 7 and 12) are all exothermic reactions, which release the energies of 24.473 kcal/mol and 19.453 kcal/mol, respectively.

These results demonstrate that the behavior of chemical dissociation from molecular hydrogen into hydrogen atoms on Al_nPt (n = 1—12) clusters can be tuned by changing the number of Al atoms, and it supports the concept of a superatom that can be used to design new nanoscale catalysts with desirable properties.

CONCLUSIONS

We have performed extensive studies on the growth behavior of Al_nPt (n = 1—12) and the H_2 adsorption and dissociation on the above mentioned clusters employing density functional calculations. The results are summarized below.

(1) The growth pattern for the Al_nPt (n = 2—4, 7, 8, and 12) clusters is the Pt atom occupying a peripheral position of the Al_n clusters [33c]. The growth pattern for the Al_nPt (n = 10 and 11) clusters is the Pt-substituted Al_{n+1} clusters. It is found that the Pt atom substitutes for the surface atom of the Al_{n+1} cluster and occupies a peripheral position.

(2) H_2 is easily physically absorbed on the top Pt atom of the Al_nPt (n = 1—12) clusters with an end-on orientation rather than a side-on orientation because of the more effective orbital overlap in the end-on orientation.

(3) The reaction of Al_nPt with H_2 would produce Al_nPtH_2 because of large exothermic energy changes and relatively small activation energies especially for Al_7Pt and $Al_{12}Pt$, which might serve as highly efficient and low-cost catalysts for the hydrogen dissociation.

(4) The conventionally adsorbed configurations with two H atoms sitting on the top of the opposite or neighboring Al atoms are found for Al_nPt (n = 4, 7—12). Three new alternative configurations are also found. One H atom is located at the bridge site and another H on the top site that is the most favorable chemisorption site for Al_5Pt and Al_6Pt clusters. Two H atoms bound on the Pt top sites are the most stable structures of $AlPtH_2$ and Al_2PtH_2, while the lowest energy geometry of Al_3PtH_2 is two H atoms binding the top site of one Al atom of Al_3Pt.

(5) By comparing the Δ_2E values for Al_nPt and Al_nPtH_2, we can state that both values follow the same trend. The particularly prominent maxima of Δ_2E of pure Al_nPt are found at n = 2, 7, and 11, indicating higher stability than that of their neighboring clusters. In the case of Al_nPtH_2, the cluster sizes n = 2 and 7 are the most stable ones.

This work was financially supported by the Natural Science Foundation of Shanxi (Grant No. 2013011009-6), the High School 131 Leading Talent Project of Shanxi, Undergraduate Training Programs for Innovation and Entrepreneurship of Shanxi Province (Grants No. 2013145 and 2015537) and Shanxi Normal University (SD2013CXCY-65) and Teaching Reform Project of Shanxi Normal University (SD2013JGXM-51).

REFERENCES

1. *Mizukoshi Y., Fujimoto T., Nagata Y., Oshima R., Maeda Y.* // J. Phys. Chem. B. – 2000. – **104**. – P. 6028 – 6032.
2. *Harikumar K.R., Ghosh S., Rao C.N.R.* // J. Phys. Chem. A. – 1997. – **101**. – P. 536 – 540.
3. *Templeton A.C., Wuelfing W.P., Murray R.W.* // Acc. Chem. Res. – 2000. – **33**. – P. 27 – 36.
4. *Whetten R.L., Shafigullin M.N., Khoury J.T., Schaaff T.G., Vezmar I., Alvarez M.M., Wilkinson A.* // Acc. Chem. Res. – 1999. – **32**. – P. 397 – 406.
5. *Christensen C.H., Norskov J.K.* // J. Chem. Phys. – 2008. – **128**. – P. 182503 – 182503-8.
6. *Tao F., Grass M.E., Zhang Y.W., Butcher D.R., Renzas J.R., Liu Z., Chung J.Y., Mun B.S., Salmeron M., Somorjai G.A.* // Science. – 2008. – **322**. – P. 932 – 934.
7. *Ma Y.G., Balbuena P.B.* // J. Phys. Chem. C. – 2008. – **112**. – P. 14520.
8. *Lovvik O.M., Opalka S.M.* // Surf. Sci. – 2008. – **602**. – P. 2840 – 2844.
9. *Soto-Verdugo V., Metiu H.* // Surf. Sci. – 2007. – **601**, N 23. – P. 5332 – 5339.
10. *Li W.Z., Liang C.H., Zhou W.J., Qiu J.S., Zhou Z.H., Sun G.Q., Xin Q.* // J. Phys. Chem. B. – 2003. – **107**, N 26. – P. 6292 – 6299.
11. *Babu P.K., Tong Y.Y., Kim H.S., Wieckowski A.* // J. Electroanal. Chem. – 2002. – **524**. – P. 157 – 167.
12. *Li H.Q., Xin Q., Li W.Z., Zhou Z.H., Jiang L.H., Yang S.H., Sun G.Q.* // Chem. Commun. – 2004. – N 23. – P. 2776 – 2777.
13. *Paulus U.A., Wokaun A., Scherer G.G., Schmidt T.J., Stamenkovic V., Radmilovic V., Markovic N.M., Ross P.N.* // J. Phys. Chem. B. – 2002. – **106**, N 16. – P. 4181 – 4191.
14. *Savadogo O., Lee K., Oishi K., Mitsushima S., Kamiya N., Ota K.I.* // Electrochem. Commun. – 2004. – **6**, N 2. – P. 105 – 109.
15. *Fernandez J.L., Walsh D.A., Bard A.J.* // J. Am. Chem. Soc. – 2005. – **127**, N 1. – P. 357 – 365.
16. *Jennings P.C., Pollet B.G., Johnston R.L.* // J. Phys. Chem. C. – 2012. – **116**. – P. 15241−15250.
17. *Peng D.L., Hihara T., Sumiyama K.* // J. Mag. Mag. Mat. – 2004. – **277**, N 1. – P. 201 – 208.
18. *Benguedouar Y., Keghouche N., Belloni J.* // Sci. and Engineer. B. – 2012. – **177**, N 1. – P. 27 – 33 .
19. *Ge Q., Song C., Wang L.* // J. Comput. Mater. Sci. – 2006. – **35**, N 3. – P. 247 – 253.
20. *Huang Y.W., Chou T.Y., Yu G.Y., Lee S.L.* // J. Phys. Chem. C. – 2011. – **115**, N 18. – P. 9105 – 9116.

21. *Chen W., Schmidt D., Schneider W.F., Wolverton C.* // J. Phys. Chem. C. – 2011. – **115**, N 36. – P. 17915 – 17924.
22. *Ishikawa Y., Diaz-Morales R.R., Perez A., Vilkas M.J., Cabrera C.R.* // J. Chem. Phys. Lett. – 2005. – **411**, N 4. – P. 404 – 410.
23. *Piotrowski M.J., Piquini P., Zeng Z.H., Da Silva J.L.F.* // J. Phys. Chem. C. – 2012. – **116**. – P. 20540 – 20549.
24. *Tarakeshwar P., Dhilip Kumar T.J., Balakrishnan N.* // J. Chem. Phys. – 2009. – **130**. – P. 114301-1—9.
25. *Huang H.S., Wang X.M., Zhao D.Q., Wu L.F., Huang X.W., Li Y.C.* // J. Acta. Phys. Sin. – 2012. – **61**, N 7. – P. 073101.
26. *Frisch M.J., Trucks G.W., Schlegel H.B., Scuseria G.E., Robb M.A., Cheeseman J.R., Vreven T., Kudin K.N., Burant J.C., Millam J.M., Iyengar S.S., Tomasi J., Barone V., Mennucci B., Cossi M., Scalmani G., Rega N., Petersson G.A., Nakasuji H., Hada M., Ehara M., Toyota K., Fukuda R., Hasegawa R., Ishida M.J., Nakajima T., Honda Y., Kitao O., Nakai H., Klene M., Li X., Knox J.E.R., Hratchian H.P., Cross J.B., Adamo C., Jaramillo J., Gomperts R., Stratmann R.E., Yazyev O., Austin A.J., Cammi R., Pomelli C., Ochterski J.W., Ayala P.Y., Morokuma K., Voth G.A., Salvador P., Dannenberg J.J., Zakrzewski V.G., Dapprich S.S., Daniels A.D., Strain M.C., Farkas O., Malick D.K., Rabuck A.D., Raghavachari K., Foresman J.B., Ortiz J.V., Cui Q., Baboul A.G., Clifford S., Cioslowski J., Stefanov B.B., Liu G., Liashenko A., Piskorz P., Komaromi I., Martin J.A., Fox D.J., Keith T., Al-Laham M.A., Peng CY., Nanayakkara A., Challacombe M., Gill P.M.W., Johnson B.G., Chen W., Wong M.W., Gonzalez C., Pople J.A.* Gaussian 03 (Revision C02); Gaussian., Inc.: Pittsburgh., PA., 2003.
27. *Becke A.D.* // J. Chem. Phys. – 1993. – **98**. – P. 5648-1.
28. *Peng C., Ayala P.Y., Schlegel H.B., Frisch M.J.* // J. Comput. Chem. – 1996. – **17**, N 1. – P. 49 – 56.
29. (a) *Gonzalez C., Schlegel H.B.* // J. Chem. Phys. – 1989. – **90**. – P. 2154. (b) *Gonzalez C., Schlegel H.B.* // J. Phys. Chem. – 1990. – **94**, N 14. – P. 5523 – 5527.
30. (a) *Chuang F.C., Wang C.Z., Ho K.H.* // Phys. Rev. B. – 2006. – **73**, N 12. – P. 125431-1. (b) *Aguado A., Lopez J.M.* // J. Chem. Phys. – 2009. – **130**. – P. 064704-1. (c) *Rao BK., Jena P.* // J. Chem. Phys. – 1999. – **111**. – P. 1890. (d) *Zope R.R., Baruah Tunna* // Phys. Rev. A. – 2001. – **64**, N 5. – P. 053202-1.
31. (a) *Cheng X.H., Ding D.J., Yu Y.G., Jin M.X.* // Chin. J. Chem. Phys. – 2012. – **25**. – P. 169 – 176. (b) *Chen M.X., Yan X.H., Wei S.H.* // J. Phys. Chem. A. – 2007. – **111**, N 35. – P. 8659 – 8662. (c) *Guo L.* // J. Alloy Copm. – 2008. – **466**. – P. 463 – 470. (d) *Gorbunov V.A., Kurkina L.I.* // Bulletin of the Russian Academy of Science: Physics. – 2008. – **72**, N 4. – P. 515 – 519.
32. *Jin R., Zhang S., Zhang Y., Huang S., Wang P., Tian H.* // Int. J. Hydrogen Energy. – 2011. – **36**, N 15. – P. 9069 – 9078.
33. *Lu Wang., Zhao J., Zhou Z., Zhang S.B., Chen Z.* // J. Comput. Chem. – 2009. – **30**, N 15. – P. 2509 – 2514.
34. *Lu Q.L., Wan J.G.* // J. Chem. Phys. – 2010. – **132**. – P. 224308-1.
35. *Parr R.G., Yang W.* Density Functional Theory of Atoms and Molecules. – New York: Oxford University Press, 1989.
36. *Parr R.G., Pearson R.G.* // J. Am. Chem. Soc. – 1983. – **105**, N 26. – P. 7512 – 7516.